Polymer Degradation and Stability 97 (2012) 421–429

Contents lists available at SciVerse ScienceDirect

Polymer Degradation and Stability

journal homepage: www.elsevier.com/locate/polydegstab

Transient temperatures of wet and dry polymeric film coated specimens experiencing outdoor exposure

William C. Thomas [a], Christopher C. White [b,*], Walter E. Byrd [b], Kar Tean Tan [b]

[a] Mechanical Engineering Department, Virginia Polytechnic Institute and State University, USA
[b] Engineering Laboratory, National Institute of Standards and Technology, USA

ARTICLE INFO

Article history:
Received 24 February 2011
Received in revised form
22 November 2011
Accepted 30 November 2011
Available online 8 December 2011

Keywords:
Organic coatings
Temperature prediction
Outdoor exposure
Degradation
Weathering

ABSTRACT

A mathematical model based on an "aggregated-capacity" temperature analysis is presented and validated for predicting the temperature of thin polymeric films bonded to substrate materials. This model is applicable to coatings on metallic or other substrate materials when the ratio of the thermal resistance across the substrate to the resistance across the coating to ambient is less than approximately 0.1. An analytical rather than a numerical method, was employed to circumvent formulation difficulties and calculation constraints associated with the latter approach for extremely thin coatings. Periodic measurements of ambient dry-bulb and dew-point temperature, wind speed (to estimate convection coefficients), sky temperature, precipitation, and solar irradiation are inputs for determining heat exchange at coating surfaces. In addition to convection and solar irradiation, the model accounts for the effects of infrared exchange with the surrounding sky, dew formation on coating surfaces, and precipitation along with insulation and ambient convection at the back surface of the substrate. Based on comparisons with National Institute of Standards and Technology data on specimen temperature and simultaneous weather data compiled between 2006 and 2008, the analytical model correlated well to measured temperatures, and provided a tractable, computationally efficient, and validated solution for predicting long term transient temperatures in thin-coated specimens.

Published by Elsevier Ltd.

1. Introduction

Organic polymeric coatings are pervasive in many applications, ranging from sports protection equipment to automotive industry, Susceptibility of these coatings to environmental factors is a primary limitation in the performance of these materials, which often leads to premature device failure [1–4]. Solar radiation (especially the ultraviolet (UV) component), elevated temperatures, moisture sorption (from ambient air and precipitation), and atmospheric particulates (such as salt) are important factors in the service life of organic coating materials. Although UV radiation is generally accepted as a primary degradation agent, humidity and temperature are also critical accelerants [1,5,6]. Work in this laboratory has shown that temperature-enhanced photodegradation of styrene-ethylene-butylene-styrene block copolymer at 55 °C/0% RH and 55 °C/80% RH was manifested in significantly higher initial rates of oxidation products that were approximately three and four time greater than that of the lower temperature counterparts at 30 °C [6].

In the case of outdoor conditions, ambient air temperature is often used as a metric for quantifying the severity of the exposure. However, ambient air temperature does not reflect the actual specimen temperature, which is a strong function of atmospheric parameters and physical properties of the specimens. For example, comparison of a white polymethylmethacrylate (PMMA) film and a white polyvinylchloride film exposed to the same outdoor conditions showed a film surface temperature difference of 2 °C; but placing the films in a xenon arc weathering chamber resulted in a substantial difference of 8.7 °C. In contrast, the surface temperature of a black PMMA film differed markedly from that of a black polyethylene by 15 °C when exposed outdoors; while a less dramatic difference of 2.6 °C was found in the xenon arc chamber [7]. On the basis of these observations, the discrepancy in the film surface temperature is anticipated to have a profound effect on the kinetics and mechanisms of degradation, and possibly lead to diverse aging characteristics in the specimens.

The apparent strong correlation between degradation and specimen surface temperature is undoubtedly due to the fact that weathering is essentially a surface effect. Together, these findings

* Corresponding author. National Institute of Standards and Technology, Engineering Laboratory, 100 Bureau Drive, Stop 8615, Gaithersburg, Maryland 20899, United States.
E-mail address: christopher.white@nist.gov (C.C. White).

0141-3910/$ – see front matter Published by Elsevier Ltd.
doi:10.1016/j.polymdegradstab.2011.11.012

Nomenclature

Bi	Biot Number
U	Effective surface conductance
L	Characteristic thickness
k	Thermal conductivity
h_w	Convection coefficient
V_w	Wind speed
G_{ir}	Measured infrared irradiance
T_{cs}	Coating surface temperature
T_{sky}	Effective sky temperature
σ	Stefan–Boltzmann constant
ε_c	Surface emissivity
L_s	Substrate thickness L_substrate p7
k_s	Thermal conductivity of the substrate (k_substrate p7)
T_a	Dry-bulb temperature
T_{dp}	Dew-point temperature
h_b	Convection coefficient for the back side of the substrate
T	Substrate aggregated temperature
T_i	Initial specimen temperature
t	Time
ρ	Density
C	Specific heat
T_{fs}	Temperature at the exposed water surface
α_{sf}	Solar absorptance of the exposed water film
i_{fg}	Latent heat of water
m_c''	Water transfer rate to the surface by condensation, evaporation, or precipitation
ρ_{va}, ρ_{vfs}	Water vapor densities in the ambient air and at the water surface
h_D	Convective mass transfer coefficient
α_a	Thermal diffusivity of water vapor in the ambient air
ρ_a	Density of water vapor in the ambient air (Is p_va same as p_a?)
C_{pa}	Specific heat of water vapor in the ambient air
D_{va}	Mass diffusivity of water vapor in the ambient air
$M_a M_v$	Molecular weights of air and water vapor
P_{atm}	Atmospheric pressure
P_g	Saturation pressure of water
L_f	Variable film thickness
ρ_f	Density of liquid water
Δt_{wd}	Weather data time interval
α_{sc}	Solar absorptance of the exposed coating surface
T_{sasc}	"Sol-air-sky-con" temperature

present a general and strong indication of the importance of relating chemical and physical degradation to the specimen surface temperature for more realistic description of the specimen condition and more precise degradation measurement. The scope of the present analysis is to provide an accurate temperature simulation model for predicting the temperatures of coatings under prevailing outdoor conditions. This model is intended for use in conjunction with outdoor exposures to accommodate an unlimited number of specimens without having to continuously measure the temperature of each one. Experimental techniques for measuring temperature of specimens exposed outdoors for long periods of time are well established. A more efficient approach is to record the temperatures of a limited number of "control" specimens, validate the mathematical model in terms of coating material properties, and use it to generate data for the sample set.

Previous efforts to mathematically simulate the transient temperatures of coatings include investigating the applicability of the established thermal model MOIST [8]. The latter is based on a distributive transient formulation and provides good predictions for temperature and moisture transfer in coating materials. Those authors' recommended enhancements included accounting for the effects of wind on convection, dew condensation, and rainfall. Additionally, Meyers [9] discusses heat transfer models correlations for panels exposed to the outdoors, with emphases on convection and meteorological data. He adapted a model originally developed for predicting the transient temperature of photovoltaic panels. His paper shows long term graphical comparisons with outdoor measurements. Pickett and Sargent [10] also present a relationship to correlate degradation in terms of coating temperature and radiation. They define an annual effective exposure temperature to account for the "total degradation damage" in terms of accumulated solar radiation and specimen temperatures. Finally, Schönlein *et al.* [11] present a simple equilibrium model that accounts for solar and infrared radiation and wind-induced convection. Unfortunately, the authors did not present the wind coefficient correlation. Calculated temperatures compare favorably with mean values measured over 10-min intervals.

2. Mathematical model

2.1. Overview

In this study, a previously developed thermal model [12] has been enhanced to account for effects of radiation and surface water on the transient temperature of polymeric coatings. The effects of radiation exchange with the surrounding sky are based on infrared measurements made with a pyrgeometer. Water effects include condensate formation (dew), evaporation (when applicable), and precipitation of various forms. The model accommodates climatic data averaged over time intervals ranging from 1 min to an hour. Hourly average temperatures are a primary output for thermal simulations.

The temperature of all coatings is assumed to be the same as the control coatings when measurements show significant precipitation. This simplification is based on the assumption that coating heat transfer properties, e.g., solar absorptance and emittance, do not materially affect the temperature of wetted specimens. This approach is taken as a result of the uncertainties in predicting the ensuing thermal response, the ready availability of measurements for the control samples, and rapid temperature response to impinging precipitation. Polymeric coatings are typically less than 100 μm thick and bonded to substrate materials with thicknesses on the order of 1 mm. Temperature transients and thermal storage capacity are dominated by the substrate - rather than the coating - and the composite specimens are thin enough to respond quickly to changes in weather conditions, especially precipitation in the form of rain, snow, sleet, etc. The development of a temperature prediction model for the more common weather condition of no precipitation but allowing for condensate formation and water evaporation follows. In cases with precipitation, the thermal analysis bypasses the equations immediately below and resumes with the water build- up calculation (Eq. (13)).

A significant reduction in the complexity of the transient mathematical model results from examining the relative energy storage capacity in layers comprising exposed specimens. Capacities

of thin polymeric coatings are generally negligible compared to those of the metallic substrates. The storage ratio for the specimens used in the present validation tests is approximately 1.6×10^{-5}. In cases with wetted surfaces, the storage capacity of the water film is also negligible. The relatively small thermal resistances across conventional substrates and negligible storage capacity of coatings justify the more tractable "aggregated-capacity (A-C)" analysis method to be used in this study, which has also been used in models discussed earlier. The much more complex alternative method is the conventional one-dimensional ("distributed capacity") transient model.

2.2. Aggregated-capacity thermal model

The simpler A-C (often denoted "lumped capacity") method is based on neglecting temperature gradients within the substrate and applies when the ratio of internal heat conduction resistance is much smaller than the film resistance at exposed surfaces. This ratio is characterized by the heat transfer Biot Number (Bi) for the substrate

$$Bi = \frac{UL}{k} \tag{1}$$

where U is the effective surface conductance (W °C^{-1} m^{-2}), L is a characteristic thickness (m), and k is thermal conductivity (W °C^{-1} m^{-1}). The thermal bond (contact) resistance between the coating and the substrate is generally negligible. Accounting for the coating conduction resistance, the effective surface conductance is determined from

$$\frac{1}{U} = \frac{1}{h} + \left[\frac{L}{k}\right]_{\text{coating}} \tag{2}$$

where h is the surface heat conductance. The latter comprises convection and radiation contributions

$$h = h_w + h_r \tag{3}$$

The convection coefficient h_w (W °C^{-1} m^{-2}) is a function of wind speed V_w (m s^{-1}) and a relationship by Watmuff *et al.* [13] is used.

$$h_w = [2.8 + 3V_w] \tag{4}$$

This relationship has been widely used to account for wind convection from various flat surfaces exposed to wind, including solar collectors and photovoltaic cells. It is much simpler than other correlations that are generally based on Reynolds and Raleigh Numbers. These other correlations require a characteristic length, which is difficult to determine for an array of small specimens; the above relationship is independent of a characteristic length. The ultimate justification for Eq. (4) is the comparisons of predictions and data, as shown in a following section.

The long-wave exchange between the coating surface and the ambient sky is governed by a nonlinear relationship between the coating surface temperature T_{cs} and the effective sky temperature T_{sky}. The latter is determined from measured infrared irradiance G_{ir} by

$$\sigma T_{\text{sky}}^4 = G_{ir} \tag{5}$$

where σ is the Stefan–Boltzmann constant (5.67×10^{-8} W K^{-4} m^{-2}). This heat exchange is taken into account by a radiation conductance defined as

$$h_r(T_{cs}, T_{\text{sky}}) = \varepsilon_c \sigma \left[T_{\text{sky}}^2 + T_{cs}^2\right]\left[T_{\text{sky}} + T_{cs}\right] \tag{6}$$

where ε_c is surface emissivity and absolute temperatures (K) are used. This relationship applies when specimens are near horizontal.

The nominal criterion for safely using the A-C method is $Bi \leq 0.1$. The "worst-case" scenario for examining the applicability of the A-C method, therefore, corresponds to maximum wind speed, h_w, maximum substrate thickness L_s, and the minimum thermal conductivity of the substrate k_s. Neglecting the surface resistance contribution (reciprocal of heat conductance) yields:

$$Bi < \frac{[L/k]_{\text{substrate}}}{[L/k]_{\text{coating}}}$$

The resistance ratio represented by the right side is approximately 0.04 for the present test specimens. The actual Bi, of course, is somewhat less, making an A-C model is fully applicable.

The aggregated-capacity model is developed for a composite specimen comprising a thin coating of thickness L_c bonded onto a substrate of thickness L_s as shown schematically in Fig. 1. Depending on specimen orientation and weather conditions, i.e., dew-point temperature and precipitation, a film of water may exist on the front (coated) surface. The exposed coating surface, therefore, exchanges heat by convection and condensation-evaporation with the ambient air at time-varying dry-bulb and dew-point temperatures $T_a(t)$, $T_{dp}(t)$, and wind speed $V_w(t)$; absorbs solar radiation $q''_{\text{solar}}(t)$; and exchanges long-wave radiation with the

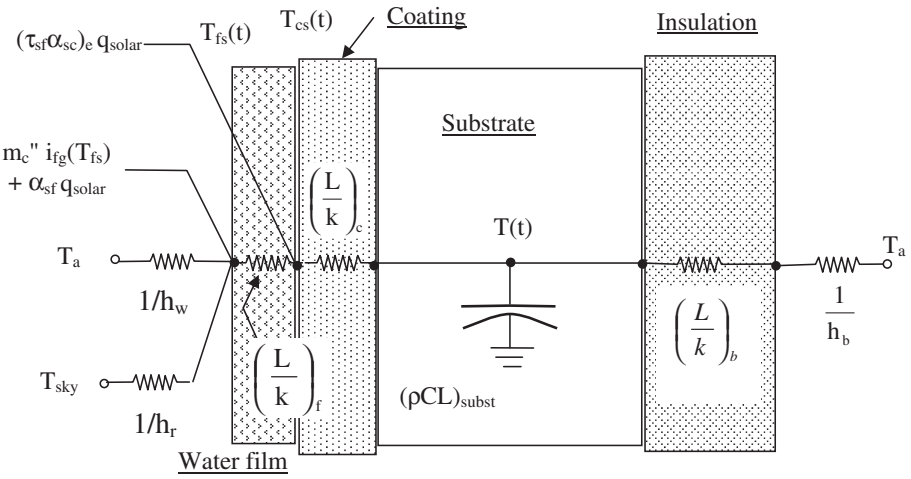

Fig. 1. Schematic of coated specimen.

ambient sky at T_{sky}. The coating is assumed opaque. The back side of the substrate may also be exposed to ambient air at $T_a(t)$ with a (different) convection coefficient $h_b(t)$ or be in contact with another layer of material, e.g., insulation.

Using the A-C approach, an energy balance for the substrate gives the governing differential equation

$$(\rho CL)_{subst}\frac{dT}{dt} = \left(\frac{k}{L}\right)_c [T_{cs}(t) - T(t)] + \left(\frac{k}{L}\right)_b [T_a(t) - T(t)]; T(0) = T_i \tag{7}$$

where $T(t)$ is the substrate aggregated temperature (°C), T_i the initial specimen temperature, t is time (s), ρ is density (kg m^{-3}), C is specific heat (J kg^{-1} °C^{-1}), k is thermal conductivity (W °C^{-1} m^{-1}), L is thickness (m), $T_a(t)$ is ambient temperature, and the subscript b denotes the back surface.

The temperature at the exposed surface of the coating $T_{cs}(t)$ differs from that of the substrate at $T(t)$. Noting that energy storage in the coating is negligible and that it may be wetted, an energy balance at the coating-water film surface is given by Equation (8).

$$T_{cs}(t) = \frac{\left(\frac{k}{L}\right)_f T_{fs} + (\tau_{sf}\alpha_{sc})_e q''_{solar} + \left(\frac{k}{L}\right)_c T(t)}{\left(\frac{k}{L}\right)_f + \left(\frac{k}{L}\right)_c} \tag{8}$$

The subscripts c and f denote the coating and water film, respectively. The effective solar transmittance through the film and absorptance at the coating surface are $(\tau_{sf}\alpha_{sc})_e$ respectively. The temperature at the exposed water surface T_{fs} is determined from the energy balance. By taking into account surface condensation-evaporation-precipitation effects, assuming that energy storage in the water is negligible, and that water is opaque for infrared radiation, the relationship is:

$$T_{fs} + \frac{i_{fg}(T_{fs})m''_c(T_{fs}) - \left[h_w T_a + h_r(T_{fs})T_{sky} + \left(\frac{k}{L}\right)_f T_{cs} + \alpha_{sf} q_{solar}\right]}{h_w + h_r + \left(\frac{k}{L}\right)_f} = 0 \tag{9}$$

where α_{sf} is the solar absorptance of the exposed water film, i_{fg} is latent heat of water, and m''_c is the water transfer rate to the surface by condensation (+) or evaporation (−) and precipitation. Condensing and evaporating rates are based on the traditional mass transfer relationship

$$m''_c = h_D[\rho_{va} - \rho_{vfs}] \tag{10}$$

where ρ_{va} and ρ_{vfs} are water vapor densities in the ambient air and at the water surface. The convective mass transfer coefficient h_D is expressed in terms of h_w using Reynolds Analogy

$$h_D = \frac{h_w}{\rho_a C_{pa}\left(\frac{\alpha_a}{D_{va}}\right)^{2/3}} \tag{11}$$

where α_a, ρ_a, C_{pa}, and D_{va} are thermal diffusivity, density, specific heat, and mass diffusivity of water vapor in the ambient air. Using the ideal gas equation of state for the densities of air and water vapor and substituting Eq. (11) into Eq. (10), the condensate flux expression is

$$m''_c(T_{fs}) = \frac{M_v h_w T_a}{M_a C_{pa} P_{atm}\left(\frac{\alpha_a}{D_{va}}\right)^{2/3}}\left[\frac{P_g(T_{dp})}{T_a} - \frac{P_g(T_{fs})}{T_{fs}}\right] \tag{12}$$

where M_a and M_v are the molecular weights of air and water vapor, P_{atm} is atmospheric pressure, and P_g is the saturation pressure of water. (The bracketed term indicates that condensation begins at a surface temperature lower than the ambient dew-point temperature. This variance is a result of modeling moisture transfer in a nonisothermal situation using density difference rather than an alternative form (e.g. in terms of water vapor-pressure difference.)

Taking the water deposited on the coating surface to be a uniform film, the accumulation is given by

$$m''_f(t) = \int_0^t m''_c(\zeta)d\zeta \tag{13}$$

where m''_c is from Eq. (12) under condensing or evaporating conditions and interpreted as precipitation rates from weather data. Clearly, not all the water deposited remains on the surface until it evaporates. Depending upon the design and orientation of the test specimens, there is likely a maximum thickness $L_{f,max}$ so the variable film thickness $L_f(t)$ can be estimated from

$$L_f(t) = \min\left(m''_f(t)/\rho_f, L_{f,max}\right) \tag{14}$$

where ρ_f is the density of liquid water. Taking the ambient weather variables constant during each weather data time interval Δt_{wd}, Eqs. (7)–(9) and Eqs. (12)–(14) can be solved for the six dependent variables. The solution algorithm must account for the effect of precipitation as described earlier, the onset of condensation in terms of dew-point temperature, and surface dry out by evaporation or run off ($L_f = 0$). The coefficient h_r is maintained constant during each time interval by basing it on mean surface (T_{csm}) and substrate (T_m) temperatures and using an iterative calculation procedure. A "stickiness" parameter is needed to avoid convergence problems when the condensation begins or surface wetting ends during a time interval.

The solution results which follow are based on a closer examination of the wetted layer as related to the specimen orientation and the actual temperature data. The specimens of interest are oriented at least a few degrees from horizontal to promote cleaner surfaces and none have protruding edges that would interfere with drainage. Furthermore, the temperature data show negligible evaporative cooling after periods of rainfall or condensate formation. Based on these and direct observation, water deposits are assume to run off immediately so the cooling effect of the film layer is neglected. Condensate forms, as predicted by Eq. (12), heats the surface as a result of phase change, and runs off with no lingering evaporative effect. In the case of precipitation, specimen temperatures revert to those measured for the control samples, as previously noted, and the water formed is assumed to run off immediately. The ultimate justification is the agreement between predicted and measured results, which are shown later.

With the absence of the water layer shown in Fig. 1, solar absorptance, infrared exchange with the sky, and ambient convection occur directly on the coating surface. Additionally, when the surface is somewhat below the dew-point temperature of the air, vapor condenses on the surface (and immediately runs off). The coatings are assumed gray surfaces for infrared radiation exchange with the sky. An energy balance on the coating surface for this situation gives

$$T_{cs}(t) = \frac{h_w T_a + h_r(T_{cs}) T_{sky} + \left(\frac{k}{L}\right)_c T(t) + \alpha_{sc} q_{solar} + m_c''(T_{cs}) i_{fg}(T_{cs})}{h_r + h_w + \left(\frac{k}{L}\right)_c} \tag{15}$$

where the term $(\tau_{sf}\,\alpha_{sc})_e$ is replaced by the solar absorptance of the exposed coating surface α_{sc}. Substituting the right hand side into Eq. (7) and rearranging gives the differential equation

$$\frac{dT}{dt} + \frac{\left(\frac{k}{L}\right)_c [h_r(T_{cs}) + h_w] + U_b\left[\left(\frac{k}{L}\right)_c + h_r(T_{cs}) + h_w\right]}{(\rho CL)_{substr}\left[\left(\frac{k}{L}\right)_c + h_r(T_{cs}) + h_w\right]} T(t) = \left[U_b T_a + \frac{\left(\frac{k}{L}\right)_c \left[h_w T_a + h(T_{cs}) T_{sky} + \alpha_{sc} q_{solar} + m_c'' i_{fg}(T_{cs})\right]}{\left[\left(\frac{k}{L}\right)_c + h_r(T_{cs}) + h_w\right]}\right] \times \frac{1}{(\rho CL)_{substr}} \tag{16}$$

This equation can be integrated for each weather data time step assuming that h_r, m_c'' and i_{fg} are constant at their mean values over a calculation time step $\Delta t \le \Delta t_{wd}$. From Eq. (15), the mean coating surface temperature is

$$T_{csm}(t) = \frac{h_w T_a + h_r(T_{csm}) T_{sky} + \left(\frac{k}{L}\right)_c T_m(t) + \alpha_{sc} q_{solar} + m_c''(T_{csm}) i_{fg}(T_{csm})}{h_r + h_w + \left(\frac{k}{L}\right)_c} \tag{17}$$

where $T_m(t)$ is the mean substrate temperature over Δt. Using the above caveat, the result of integrating Eq. (16) is

$$\begin{aligned} T(t) &= [T_i - T_{sasc}]\exp(-t/\tau_c) + T_{sasc} \\ \tau_c &= \frac{(\rho LC)_{subst}\left[\left(\frac{k}{L}\right)_c + h_r(T_{csm}) + h_w\right]}{\left(\frac{k}{L}\right)_c [h_r(T_{csm}) + h_w] + U_b\left[\left(\frac{k}{L}\right)_c + h_r(T_{csm}) + h_w\right]} \\ T_{sasc} &= \frac{\left\{U_b\left[\left(\frac{k}{L}\right)_c + h_r(T_{csm}) + h_w\right] + \left(\frac{k}{L}\right)_c h_w\right\} T_a + \left(\frac{k}{L}\right)_c \left[h_r(T_{csm}) T_{sky} + \alpha_{sc} q_{solar} + m_c'' i_{fg}(T_{csm})\right]}{\left(\frac{k}{L}\right)_c [h_r(T_{csm}) + h_w + U_b] + U_b [h_r(T_{csm}) + h_w]} \end{aligned} \tag{18}$$

where T_i is the substrate temperature at the beginning of each time step. T_{sasc} may be denoted the "sol-air-sky-con" temperature, and would be the equilibrium temperature for a specimen exposed to ambient air and sky temperatures, solar irradiance, and condensate formation. Note that T_{sasc} is also the temperature of a specimen with negligible energy storage capacity.

The mean substrate temperature during a time interval t is

$$T_m(t) = \frac{1}{t}\int_0^t T(\zeta)\,d\zeta = T_{sasc} + [T_i - T_{sasc}]\frac{\left[1 - \exp\left(-\frac{t}{\tau_c}\right)\right]}{\frac{t}{\tau_c}} \tag{19}$$

2.3. Simulation procedure

Calculations to simulate transient temperatures comprise four nested loops. Since hourly average temperatures are an objective, the algorithm comprises an outer (hourly) loop with an inner loop to read the weather data for each measurement interval. The data are checked first for precipitation and then for dew formation, based on the bracketed term in Eq. (12) being positive. In the next inner loop, the weather data intervals Δt_{wd} are divided into subinterval time steps Δt. Eqs. (17) and (19) are solved simultaneously using Newton–Raphson iteration in the innermost loop. Eq. (18) gives temperature at the end of each step which is the initial temperatures for the next step. The time response parameter τ_c (analogous to a "time constant") and T_{sasc} are updated for each step. The procedure is repeated for each weather data interval with smaller time steps until values of T_m and T_{csm} converge during the last steps in the data intervals. If needed, the final calculation time step is 60 s. At the end of each hour the interval means are averaged for hourly means. The mean temperature over several consecutive measurement intervals, e.g., for an hour, is the average of the individual means.

The solution algorithm has been implemented as a Visual Basic for Applications™ (VBA) module in an Excel™ spreadsheet. Weather data is copied to a worksheet, input parameters and calculated results are on another worksheet, and spreadsheet plots show results graphically. The final Excel program that incorporates the iterative procedure is designated PFTemp.xls version 9.

Calculation time for simulating hourly average temperatures of specimens for a year is typically on the order of seconds, depending somewhat on the weather duration interval and calculation time step.

3. Validation of model

Predictions are compared with data provided by NIST from their test facility located in Gaithersburg, MD. The specimens are mounted as shown in Fig. 2 on the roof of Building 226. The outdoor conditions measured include ambient dry-bulb temperature, relative humidity, precipitation (rainfall), sky and solar radiation, wind speed and direction, and barometric pressure.

Temperatures sensors are thermocouples. Solar and sky radiation are measured using precision pyranometer and pyrgeometer instruments mounted horizontally. Wind speed and direction are measured by an adjacent anemometer located approximately 0.3 m above the specimen surfaces. A film-type humidity sensor measures relative humidity; dew-point temperatures are calculated. (Weather data is also available from the NIST BIP Weather Station that is located about 75 m away on the same roof. Data from the two sources agree well and supplement each other during outages.)

3.1. Specimens and properties

Test specimens comprise a 20 gauge aluminum substrate (approximately 1/32 in. or 0.8 mm thick) with a specially prepared

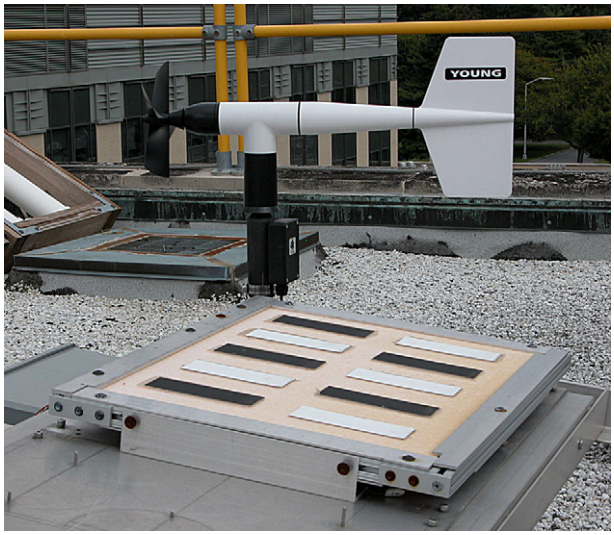

Fig. 2. Specimen exposure setup.

coating of latex paint on the exposed surface. The coating is 20 μm thick, as measured by the paint manufacturer. Five specimens of the array have black paint and 5 have white paint. Each specimen is 5.4 in. (137.2 mm) long by 1.82 in. (46.2 mm) wide. The specimens are mounted flush in a sheet of closed-cell foam plastic insulation with an estimated back side R-value of 4 $ft^2 \cdot F \cdot h/Btu$ ($R_m = 0.83\ ^\circ C\ m^2\ W^{-1}$). The assembly of 10 specimens is sloped approximately 5° - to facilitate draining – and faces south. It is exposed directly to solar irradiation, the surrounding sky, and prevailing wind. Two thermocouples sandwiched between the foam and aluminum sheet at bottom and top corners measure the temperature of each specimen.

The thermal properties of the paint material needed for the simulation model are either measured, handbook values, or estimated from test observations. The latter is used in cases where direct property measurements are not yet available. The NIST provided measurements for the total normal emittances of the paint materials using a Gier-Dunkle reflectometer. The values for the black and white paint are 0.905 and 0.869; these are taken as hemispherical properties. The solar absorptance of the white latex paint is taken as 0.26, which is a handbook value listed for "white acrylic resin" paint [14]. This reference, and others examined, did not list black latex measurements, so temperature measurements during the peak solar radiations are used to indicate an approximate value to compare trends and differences in temperatures. The remaining less critical property values were estimated from handbooks based on similar materials. For the paint film, the density, specific heat, and thermal conductivity were taken as 1200 kg m^{-3}, 1250 J $kg^{-1}\ ^\circ C^{-1}$, and 0.25 W $^\circ C^{-1}\ m^{-1}$. For the aluminum substrate, the respective values are 2700 kg m^{-3}, 903 J $kg^{-1}\ ^\circ C^{-1}$, and 238 W $^\circ C^{-1}\ m^{-1}$.

4. Results and discussion

Fig. 3 shows a plot of the relevant weather data for 29 June 2006 along with measured temperatures for two typical samples with a black paint coating. Measurements of specimen temperature and ambient conditions were made every 12 s and averages for each minute were recorded. The figure shows the 1-min insolation averages as measured along with the 15-min. averages that were generally used in the temperature simulations. This day-of-the-year (doy) 181 was relatively calm with a maximum wind speed of 1.3 m s^{-1}, had a few scattered clouds, and the relative humidity ranged from 35 % to 100 %. Note that for the first 7 h shown, specimen temperatures were less than the ambient dew-point temperature, indicating surface condensation. The lower specimen temperature is a result of the decreased sky temperature at night; the ambient dew-point is only slightly less than the ambient dry-bulb temperature, corresponding to high relative humidity.

An examination of the data at any given time for all like-color coatings shows only small temperature differences between all the specimens at both thermocouple locations (except for obvious

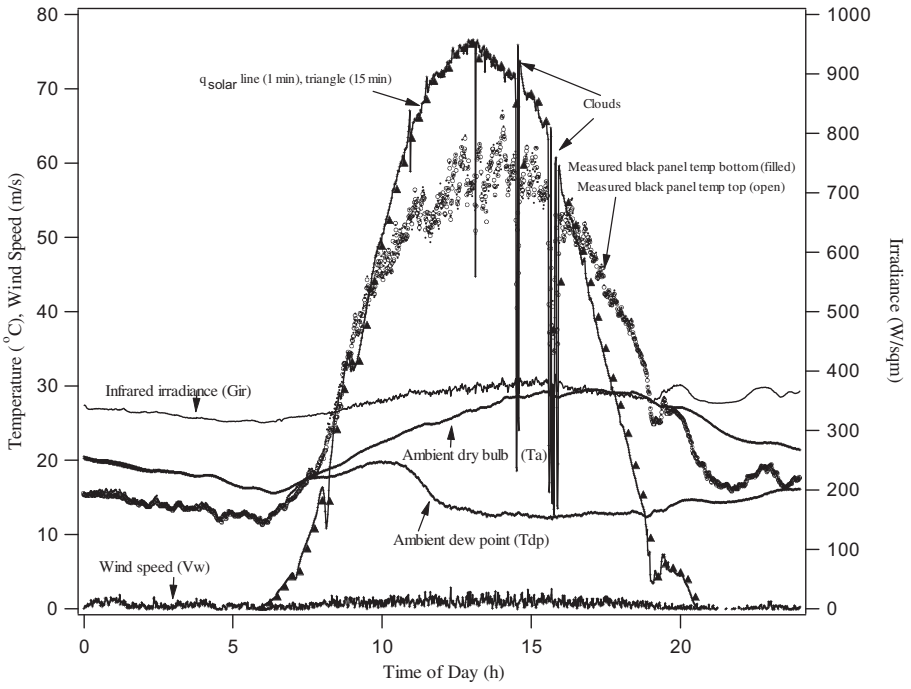

Fig. 3. Weather data for 29 June 2006 along with measured temperatures for two typical samples with a black paint coating.

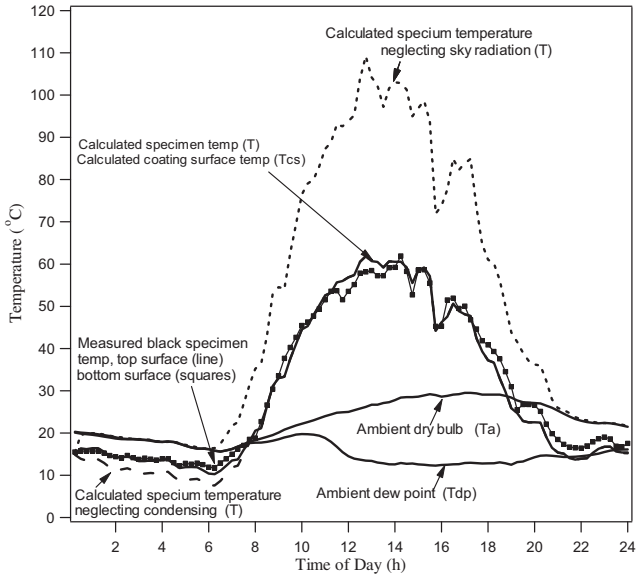

Fig. 4. Comparison of measured and predicted temperatures for a white specimen during 29 June 2006. Prediction from the equations agrees well with experimental data.

instrumentation malfunctions with white specimens (Fig. 4) and black specimen (Fig. 5). Furthermore, the figure shows that differences between the temperatures measured by the thermocouples at top and bottom corners are not significant. Considering the small differences and the significant uncertainties in the thermal properties of the coatings, comparisons of predicted and measured temperatures are shown for only two representative specimens of each color.

4.1. Comparison of predicted and measured temperatures

Fig. 4 compares the predicted mean temperature over each 15-min. interval with the measured averages over the same interval for a specimen with white paint coatings. The differences in measured temperature (squares and diamonds) at the two locations are negligibly small. For this composite specimen, the differences

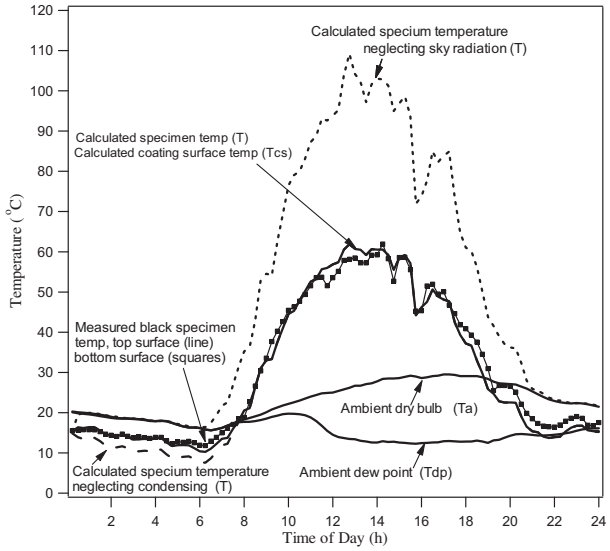

Fig. 5. Comparison of measured and predicted temperatures for a black-coated specimen exposed to the same weather conditions shown in Fig. 4.

between the temperature of the substrate and exposed coating surface are insignificant.

The agreement between measured and calculated temperatures during daylight hours is remarkably good. The close agreement between the daytime predictions and data indicate that the present paint and "acrylic resin" have about the same solar absorptance. The maximum deviation occurs after about 17 h as the specimen cools and is of the order of 3 °C.

As noted earlier in Fig. 3, condensate forms on the coating surface during the initial hours and the heating effect is taken into account in the predictions. After about 8 h, the surface temperature is higher than the ambient dew-point thus condensing ceases and any residual surface liquid would start evaporating. These and subsequently presented specimen temperature data indicate the evaporative cooling effect is small, which supports the assumption that most condensation runs off rather than evaporates on the coating surface.

Fig. 5 shows the comparisons for a black-coated specimen exposed to the same weather conditions as in Fig. 4. The predicted effects on specimen temperature of moisture condensation and sky temperature are also presented to compare capabilities of the present and earlier thermal models.

The peak measured temperatures are of necessity used as the basis for an expected value of solar absorptance, since neither a measured or handbook reference value is currently available for this black latex paint. The measured peak temperatures for the black specimen are approximately 20 °C higher than for the white specimens under the same exposures. Based on NIST data and the analytical model, the latex paint is expected to have a solar absorptance in the 0.55–0.65 range. An absorptance value of 0.6 was used for the calculated temperatures shown in the figure to examine trends and differences. The predicted temperatures follow the measurement trends of the data well using the estimated absorptance value.

The corresponding dotted line plot shows the predicted error when condensate heating (and evaporative cooling) of the specimen is neglected. When the surface is approximately 5 °C below the ambient dew-point temperature, the error is about 3 °C. Note that when the surface temperature rises above the dew-point, there is no apparent cooling effect of any residual liquid on the surface. For the weather conditions and specimens in the present investigation, surface condensing noticeably effects only predicted minimum temperatures.

The other dotted line shows that neglecting infrared radiation exchange with the sky can be highly significant. The effective sky temperature is generally less than that of the ambient air and has the greatest effect during periods of high insolation. The results show that infrared irradiance, or effective sky temperature, is an essential measurement for accurate temperature predictions.

4.2. Comparison of instantaneous and equilibrium temperatures

Some previous temperature models in the literature are based on equilibrium rather than transient formulations. The former are, of course, much simpler; T_{sasc} in Eq. (18) corresponds to the equilibrium version of the present formulation. The validity of this simplification depends on the ratio of the weather measurement interval Δt_{wd} to the response time parameter τ_c (Eq. (18)). Based on the present specimen properties and for doy 181 conditions, calculations show that τ_c ranges from 1.7 to 4.1 min.

The stacked plots in Fig. 6 compare predicted equilibrium temperatures T_{sasc}, and interval mean temperatures $T_m(t)$ with data. Referring to the upper plots and left ordinate scale, the equilibrium simplification is fully valid for the present conditions and 15-min data averages with $3.7 \leq \Delta t_{wd}/\tau_c \leq 8.8$. Referring to the lower

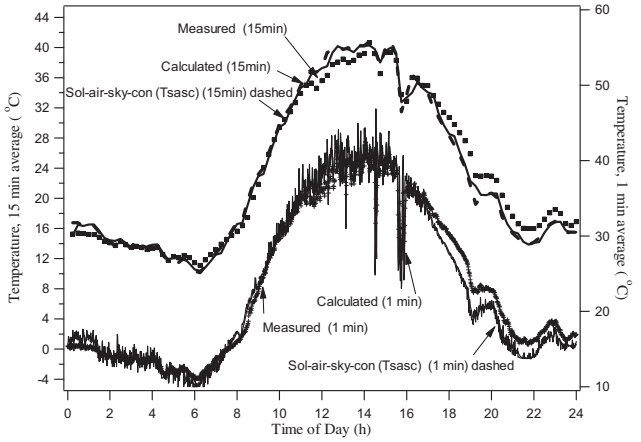

Fig. 6. Comparisons of equilibrium and transient temperatures for two weather measurement intervals (1 min averages and 15 min averages) for a white specimen during 29 June 2006. The 15 min equilibrium temperature averages agree well with the comparable measured values; while the differences for the shorter 1-min averages are slightly more pronounced.

plots and right ordinate for the shorter 1-min. averaging interval, the differences are slightly more pronounced since $0.24 \leq \Delta t_{wd}/\tau_c \leq 0.59$.

The above comparisons are with data from a relatively calm and clear day with no precipitation. Comparisons follow for a windy day with sporadic cloud cover and rain. These are to examine the applicability of wind convection correlation, Eq. (4); the assumption that all specimens exposed to precipitation reach the same temperature; and evidence of changes in coating properties after prolonged outdoor exposure.

4.3. Applicability of wind convection correlation

Fig. 7 shows the weather conditions for 18 March 2008 along with temperature data for two specimens coated with white paint. The total precipitation measured was 3.4 mm, which is not shown in the figure. The average wind speed is 8.2 m s^{-1} compared to 0.6 m s^{-1} for the day shown in Fig. 3.

Fig. 8 compares the data and calculations for a white specimen during this test day. The predicted temperatures shown are 15 min.

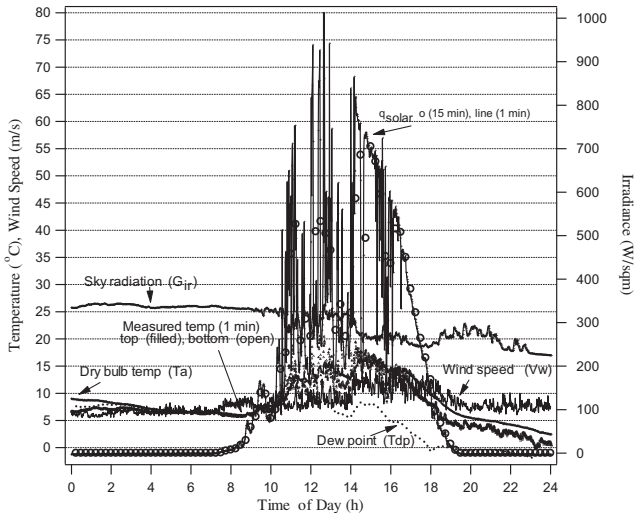

Fig. 7. Weather conditions for 18 March 2008 along with temperature data for two specimens coating with white paint.

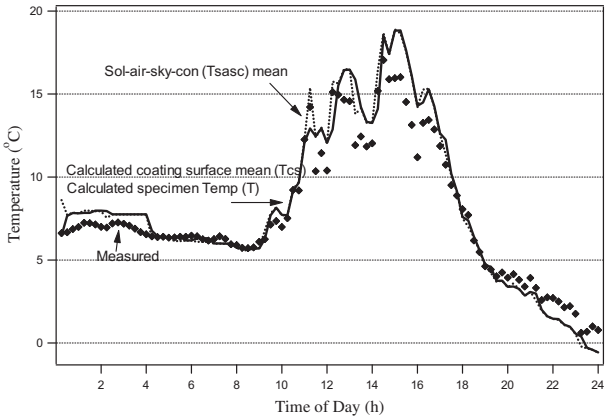

Fig. 8. Comparison of measured and predicted temperatures in 15 min averages for a white specimen during 18 March 2008. The measured and predicted temperatures are in relatively good agreement.

averages connected by smoothed lines. As expected, the specimen substrate temperature is essentially the same as the coating surface temperature. The maximum difference between predicted and measured temperatures is of the order of 3 °C. The relative agreement of measured and predicted temperature indicate that the solar absorptance and emittance of the coating surface has not changed significantly after nearly two years of continuous outdoor exposure.

Fig. 9 compares hourly averaged temperatures for the same day and specimen. Averages based on each hour are likely to be the primary results from the present model that will be used as input for research in predicting service life of coating materials. The smoothing effect of the longer time interval and somewhat better agreement with data is apparent.

Although there is more scatter in differences compared to those in Fig. 4 for a relatively calm day, overall relative agreement in the two figures with the much higher wind speed indicates the simple wind convection relationship is adequate. In both figures, the equilibrium temperature T_{sasc} agrees closely with predictions based on the transient model.

4.4. Temperatures of specimens during rain

The validity of assuming all specimens of each generic type exposed to precipitation attain the same temperature is examined in Fig. 10. Data show rainfall in the amount of 0.1 mm–0.2 mm occurred

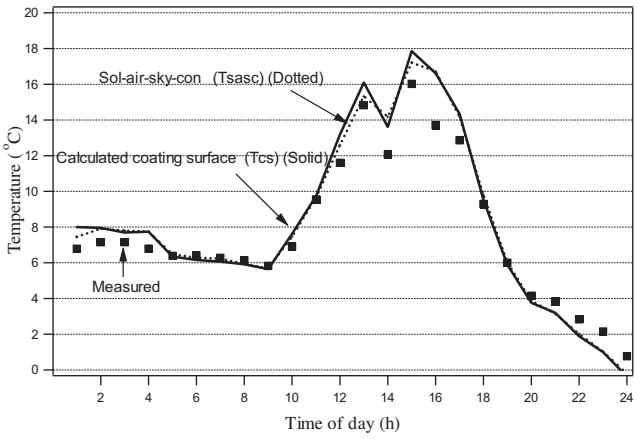

Fig. 9. Comparison of measured and predicted temperatures in hourly averages for the same day and specimen shown in Fig. 8. The smoothing effect of the longer time interval and somewhat better agreement with data is apparent.

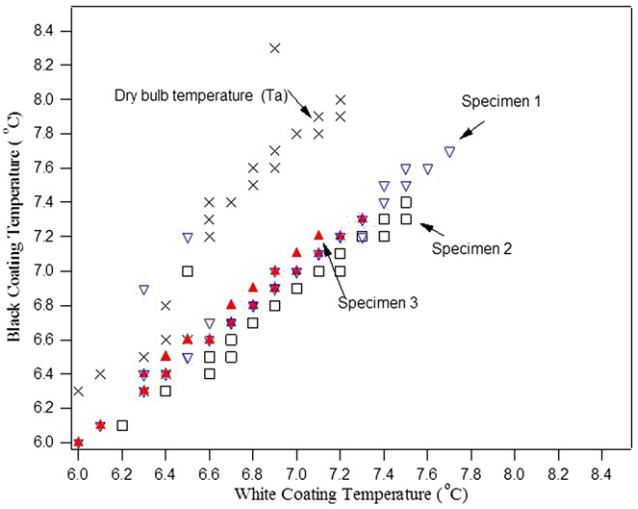

Fig. 10. Mean temperatures of three black and three white-coated samples along with the ambient dry-bulb for each period during intervals with rain. The discrepancy between the two different samples are generally within ± 0.5 °C of each other; while the sample temperatures are 1 °C–2 °C below the ambient temperature.

during 30 one-minute periods for doy 76. The measured mean temperatures of three black- and three white-coated samples along with the ambient dry-bulb for each period are cross plotted for comparison. Ideally, all data pairs would lie on the diagonal if equal. Although some outliers appear, the temperatures of the different specimens are generally within ± 0.5 °C of each other when it is raining. On the other hand, the surfaces are generally 1 °C–2 °C below the ambient temperature. These observations indicate that during periods of precipitation the temperature of exposed specimens can be safely taken as that of control samples. An alternative of assuming them to attain ambient temperature is not as accurate.

5. Discussion

The most critical uncertainties in predicting temperatures are likely to be the coating surface property values and exposure-induced changes, i.e., solar absorptance and emittance. The effects of different correlations for convection coefficients in terms of ambient wind speed and direction; various forms of precipitation; and evaporation also merit additional investigations. The condensate heating effect is only significant for predicting temperatures below the ambient dew-point temperature. It is included in the present model to establish its significance. The present investigation advances the state-of-the-art in predicting temperatures of thin organic coatings relative to the thermal aspects of service life research. Feedback from material researchers is needed as a guide for future enhancements and refinements to the mathematical model.

6. Conclusions

A tractable mathematical model based analytical relationships for comprising components of composite specimens is presented. The closed-form solution is computationally efficient for predicting transient temperatures in thin-coated specimens. The thermal model accounts for effects on coating temperature of ambient air temperatures; wind-induced convection; infrared sky radiation; solar radiation; dew formation; precipitation; and thermal energy storage within the substrate material.

A simpler “aggregated-capacity” formulation was shown to apply and is used for predicting the temperature history for typical composite specimens. It is justified by the small Biot No. criterion, which was described and implemented. The criterion for using the latter, which is simpler that the transitory formulation, is presented. The equilibrium, i.e., steady-state, temperature relationship is included in the formulation. Comparisons show that the equilibrium model is applicable to the present test specimens when the weather measure interval is about 15 min, or longer.

Even with limited property and test data for the coating materials, comparisons of predictions with measurements indicate that the present mathematical model is satisfactory for supporting service life research on thin organic coatings. Results compare favorably for a calm, nearly clear 24 h day and for a windy, mostly cloudy day. An uncomplicated correlation for wind convection, independent of a characteristic dimension and air properties, is shown to be satisfactory for two significantly different wind conditions. The temperature model accounts for the heating effect of dew formation. The data support the observation that liquid water, from condensation or precipitation, runs off the (tilted) specimens surfaces quickly so that the evaporative cooling effect is negligible. The data also show that in the presence of rain, coated specimens with different heat transfer properties attain nearly the same temperature. This observation along with measurements for one or more “control” specimens is used to approximate the temperature of all test specimens in situations that are otherwise difficult to analyze.

Simulations with the model show that peak temperatures are highly dependent on the solar absorptance of surfaces and on sky radiation. Consequently, solar absorptance and surface emittance properties for the coating surface and changes resulting from long term outdoor exposure are critical material characteristics for long term simulations. A precision pyranometer and a pyrgeometer, for measuring solar and infrared radiation, are essential components of the weather station instrumentation.

References

[1] Jacques LFE. Accelerated and outdoor/natural exposure testing of coatings. Progress in Polymer Science 2000;25:1337–62.
[2] Martin JW, Nguyen T, Byrd E, Dickens B, Embree N. Relating laboratory and outdoor exposures of acrylic melamine coatings: I. Estimation of total absorbed dosage and spectral quantum yield. Polymer Degradation and Stability 2002;75:193–210.
[3] Bauer DR. Predicting in-service weatherability of automotive coatings: a new approach. Journal of Coatings Technology 1997;69:85–95.
[4] Tan KT, White CC, Benatti DJ, Hunston DL. Evaluating aging of coatings and sealants: mechanisms. Polymer Degradation and Stability 2008;93:648–56.
[5] Rabek JF. Polymer photodegradation - mechanisms and experimental methods. London: Chapman and Hall; 1995.
[6] White CC, Tan KT, Hunston DL, Nguyen T, Benatti DJ, Stanley D, et al. Laboratory accelerated and natural weathering of styrene-ethylene-butylene-styrene (SEBS) block copolymer. Polymer Degradation and Stability 2001; 96:1104–10.
[7] Schniewind BJ. Polymers Paint Colour Journal 1989;179(4250):841–7.
[8] Burch DM, Martin JW. Predicting the temperature and relative humidity of polymer coatings in the field. Service life prediction of organic coatings. American Chemical Society; 1999. pp. 85–107.
[9] Myers Daryl R. Predicting temperatures of exposure panels: models and empirical data. Service life prediction of organic coatings. American Chemical Society; 1999. pp. 71–84.
[10] Pickett JE, Sargent JR. Sample temperatures during outdoor and laboratory weathering exposures. Polymer Degradation and Stability 2009;94:189–95.
[11] Schönlein A, Haillant O, Senff S. Surface temperatures of colour painted specimen in natural and artificial weathering with different laboratory light sources for optimized testing and investigations. In: Reichert T, editor. Natural and artificial ageing of polymers. Budapest: CEEES; 2009.
[12] Thomas WC, White CW, VanLandingham MR. Moisture diffusion and temperature history models for thin organic coatings exposed to ambient air. In: Martin JW, Ryntz RA, Dickie RA, editors. Service life prediction, challenging the status quo. Federation of Societies for Coatings Technology; 2005.
[13] Watmuff JHC, Charters WWS, Proctor D. Solar and wind induced external coefficients - solar collectors. cooperation mediterraneenne pour l'Energie Solaire. Revue Internationale d'Heliotechnique; 1977. 56.
[14] American society of heating R, and air-conditioning engineers fundamentals handbook; 2005.